Characteristics of the Multiple-Input DC–DC Converter

Hirofumi Matsuo, *Fellow, IEEE*, Wenzhong Lin, Fujio Kurokawa, *Senior Member, IEEE*, Tetsuro Shigemizu, and Nobuya Watanabe

***Abstract*—In the zero-emission electric power generation system, a multiple-input dc–dc converter is useful to obtain the regulated output voltage from several input power sources such as a solar array, wind generator, fuel cell, and so forth. A new multiple-input dc–dc converter is proposed and analyzed. As a result, the static and dynamic characteristics are clarified theoretically, and the results are confirmed by experiment.**

***Index Terms*—Boundaries of stability, clean energy, dc–dc converter, multiple input, solar array.**

I. Introduction

RECENTLY, the zero-emission electric power generation system has been developed aggressively to exploit clean energy resources such as the solar array, wind generator, fuel cell, and so forth. In this case, the multiple-input dc–dc converter [1], [2] is useful to combine several input power sources whose voltage levels and/or power capacity are different and to get regulated output voltage for the load from them, as shown in Fig. 1. For example, in the solar array power supply system with a commercial ac line, the maximum power point of a solar array can be easily tracked while simultaneously the output voltage can be easily regulated by receiving adequate power from the commercial ac line, even if the load is changed.

The purpose of this paper is to propose a new multiple-input dc–dc converter for realizing the zero-emission electric power generation system. In particular, the two-input buck–boost-type converter is analyzed, and the static and dynamic characteristics are clarified theoretically and confirmed by experiment.

II. Circuit Configuration and Operation Principle

Fig. 2(a) and (b) shows the basic configuration of multiple-input dc–dc converters. Fig. 2(a) is fundamentally composed of the buck–boost-type dc–dc converter, in which multiple input windings have magnetic coupling through the energy-storage reactor *L*. Using the magnetic coupling of the isolation transformer *T*, the forward type multiple-input dc–dc converter is obtained as shown in Fig. 2(b).

Manuscript received May 24, 2002; revised June 11, 2003. Abstract published on the Internet January 14, 2004.

H. Matsuo, W. Lin, and F. Kurokawa are with the Graduate School of Science and Technology, Nagasaki University, Nagasaki 852-8521, Japan (e-mail: h-matsuo@net.nagasaki-u.ac.jp).

T. Shigemizu is with the Nagasaki Research and Development Center, Mitsubishi Heavy Industries, Ltd., Nagasaki 851-0392, Japan.

N. Watanabe is with Choryo Engineering Company, Ltd., Nagasaki 851-0392, Japan.

Digital Object Identifier 10.1109/TIE.2004.825362

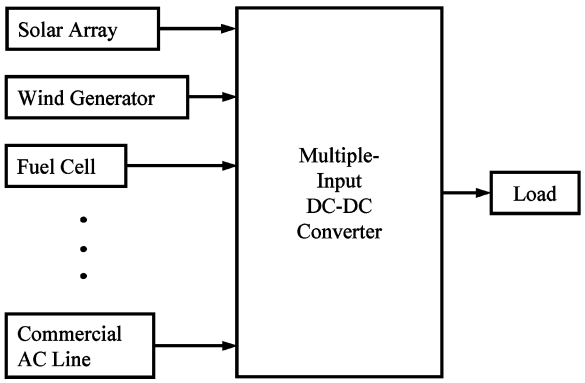

Fig. 1. Zero-emission electric power generation system using multiple-input dc–dc converter.

In this paper, the buck–boost-type two-input dc–dc converter using the coupling of reactor *L*, as shown in Fig. 3(a), is examined because a general discussion of multiple-input converter is too complicated and the buck–boost-type dc–dc converter has a simpler circuit configuration. In this figure, the two inputs E_1 and E_2 are the input voltages from two power sources, while N_1 and N_2 are the turns ratios of two input windings of the reactor. The number of turns of the output winding of the reactor is normalized and is equal to unity. S_1 and S_2 are the switches, D, D_1, and D_2 are the diodes, C is the output smoothing capacitance, R is the load, and e_o is the output voltage.

If the solar array and the commercial ac line are used as input power resources, then the circuit configuration is as shown in Fig. 3(b). The solar cell E_S, used for monitoring, and the current sensor R_S is employed to track the maximum power point of the solar array [3] which is the output current value to obtain the maximum output power from the solar array when the light intensity is varied. In this case, the commercial ac line is employed to regulate the output voltage.

Assuming that the switches and diodes have ideal characteristics, then the circuit shown in Fig. 3(a) can be divided into four states according to the combination of the on and off condition of the switches S_1 and S_2, and the diode D, as shown in Table I. The operation of the converter is determined by combining these four states, thereby being divided into three major modes as shown in Table II. Each major mode consists of a two-state sequence which is distinguished between the continuous and discontinuous reactor current modes (see Appendix I). Fig. 4 shows the waveforms of a driving signal, where T_S is the switching period, and $T_{\rm on1}$ and $T_{\rm on2}$ are the on times of the switches S_1 and S_2, respectively. As shown in Fig. 4(b), $T_{\rm off} = T_S - T_{\rm on1} - T_{\rm on2}$.

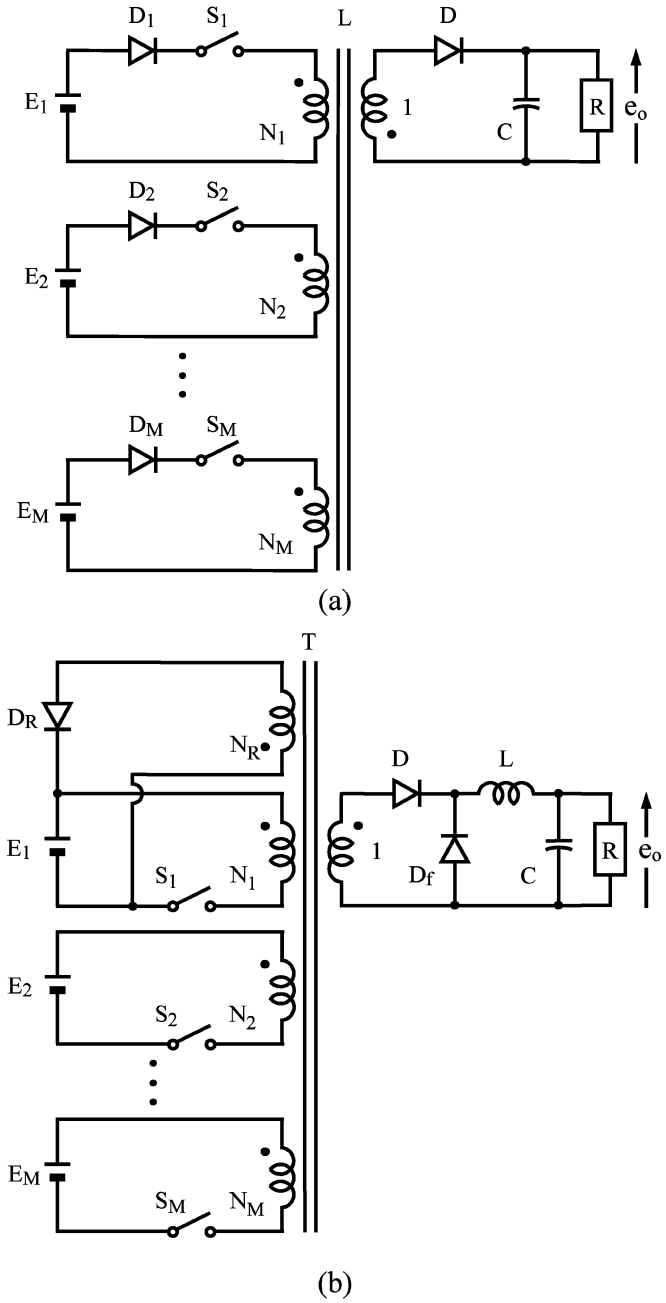

Fig. 2. Multiple-input dc–dc converter. (a) Buck–boost type using the magnetic coupling of reactor L. (b) Forward type using the magnetic coupling of transformer T.

Mode I appears under a relatively light load condition, in which the generated power of the solar array is larger than the load power and the maximum power point of the solar array is not tracked. As a matter of course, if a battery system is used to store the excess energy of the solar array, its maximum power point may be tracked. In Mode II, S_1 is used to perform the optimum power point control of E_1 and S_2 is used to regulate the output voltage E_o. Mode III appears when the solar array does not generate the output power, or $E_1 = 0$ because the light intensity for the solar array is too weak in Fig. 3(b).

In Modes I and III, the proposed two-input buck–boost-type dc–dc converter operates as a conventional single-input converter since the input power source is E_1 or E_2. Therefore, we

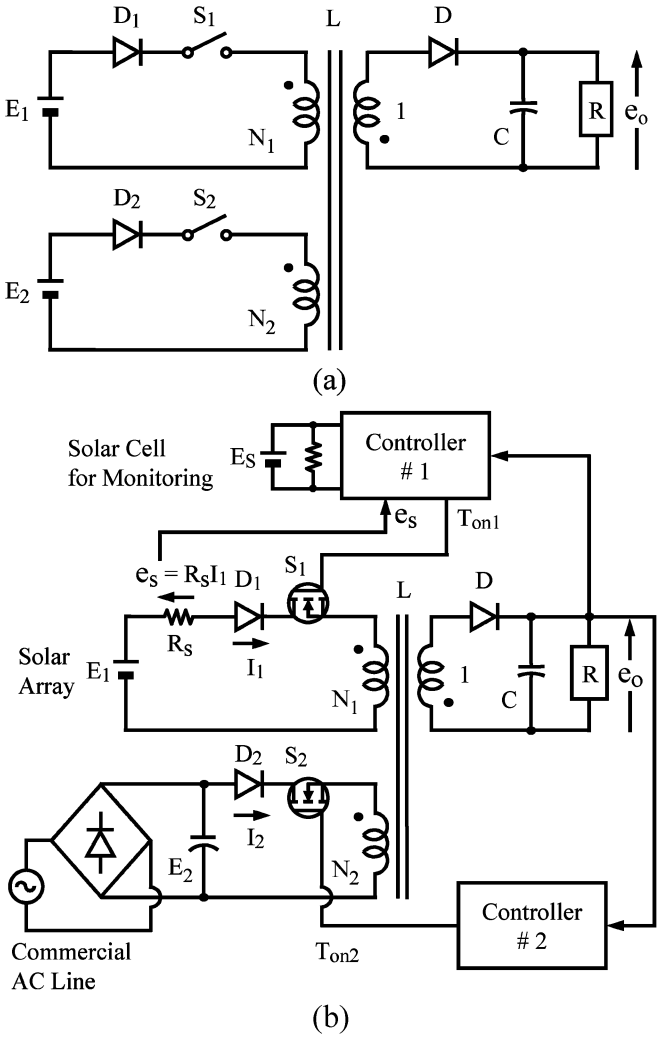

Fig. 3. (a) Buck–boost-type two-input dc–dc converter. (b) Two-input dc–dc converter using a solar array and a commercial ac line.

discuss mainly Mode II shown in Fig. 4(b), in which two inputs must be considered.

III. Analysis of Static and Dynamic Characteristics

A. Equivalent Circuit Models

Before discussing the characteristics of the two-input dc–dc converter, as shown in Fig. 3(a), the following assumptions will be made.

1) The switches S_1 and S_2 have internal resistance r_{S1} and r_{S2} and diodes D, D_1, and D_2 have internal resistance r_D, r_{D1} and r_{D2}, respectively.
2) The respective switching time of S_1, S_2 and D are sufficiently shorter than the on-time interval $T_{\rm on1}$, $T_{\rm on2}$ and the off-time interval $T_{\rm off}$, so that they can be neglected.
3) Energy-storage reactor L has ideal magnetic characteristics and, hence, no leakage flux exists among the windings of L.
4) The inductance of energy-storage reactor L is large enough to make the magnetomotive force (MMF) of the reactor continuous, i.e., the converter operates in the continuous reactor current mode shown in Table II.

TABLE I
STATES OF BEHAVIOR

State	S_1	S_2	D
1	on	off	off
2	off	on	off
3	off	off	on
4	off	off	off

TABLE II
OPERATION MODES AND STATE SEQUENCES

Mode	State Sequences	
	Continuous	Discontinuous
I	1→3→1	1→3→4→1
II	1→2→3→1	1→2→3→4→1
III	2→3→2	2→3→4→2

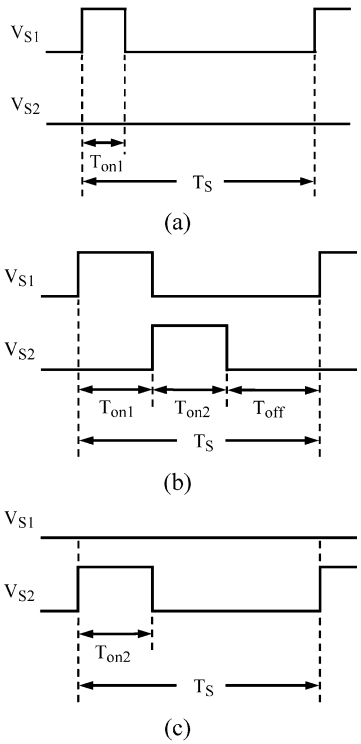

Fig. 4. Waveforms of driving signal in each mode, corresponding to Tables I and II. (a) Mode I. (b) Mode II. (c) Mode III.

Given the above assumptions, equivalent circuit models [3] of three states, except State 4 in Table I, are shown in Fig. 5. In this figure, the ideal transformer is used to represent the two-input dc–dc converter by the equivalent circuits with the same circuit topology. In Fig. 5, the input voltages E_1 and E_2 are normalized by the number of turns of the two primary windings N_1 and N_2 of the reactor L. As a result, they are represented by E_1/N_1 and E_2/N_2. The on-state and off-state of the S_1 and S_2 are represented by turns ratios of 1:1 and 1:0 in the ideal transformer, respectively. Similarly, the on-state and off-state of D are represented by turns ratios of 1:1 and 0:1 in the ideal

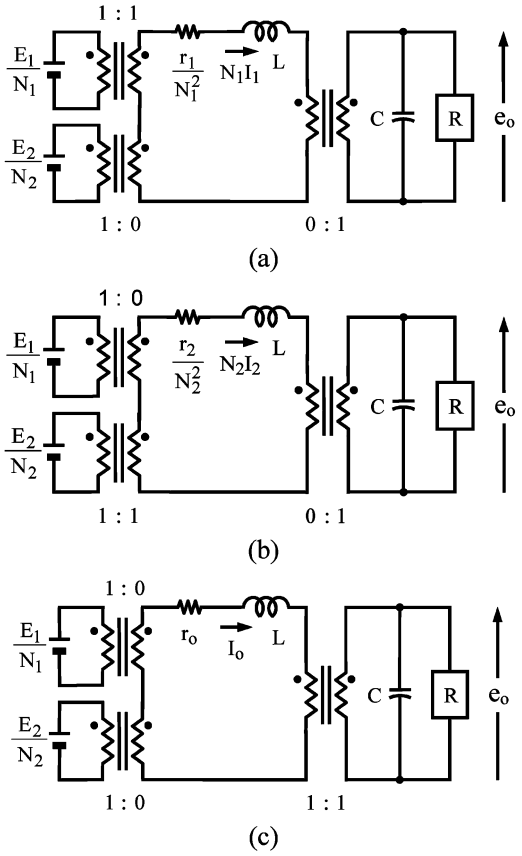

Fig. 5. Equivalent circuits with ideal transformer, corresponding to Table I. (a) State 1. (b) State 2. (c) State 3.

transformer, respectively. As shown in Table I, in State 1, S_1 is on, S_2 is off, and D is off. In this state, the current N_1I_1 flows from E_1/N_1 to the primary winding N_1 of the reactor L shown in Fig. 5(a). In State 2, S_1 is off, S_2 is on, and D is off, and then N_2I_2 flows from E_2/N_2 to the primary winding N_2 of L shown in Fig. 5(b). In State 3, S_1 is off, S_2 is off, and D is on, and therefore I_o flows from the secondary winding of L to the load R connected with the output capacitor C in parallel. r_1, r_2, and r_o are given by

$$r_1 = r_{E1} + R_S + r_{S1} + r_{D1} + r_{L1} \tag{1}$$

$$r_2 = r_{E2} + r_{S2} + r_{D2} + r_{L2} \tag{2}$$

$$r_o = r_D + r_{Lo} \tag{3}$$

where r_{E1} and r_{E2} are the internal resistances of E_1 and E_2, R_S the series current-sensing resistance, and r_{L1}, r_{L2}, and r_{Lo} the internal resistance of the two input windings and an output winding of the reactor L, respectively.

Using the equivalent circuit models in Fig. 5, the continuous equivalent circuit models [4] averaged over a single switching period T_S are derived as shown in Fig. 6 [see Appendix II], where r represents the equivalent internal loss resistance and is given by

$$r = \frac{T_{\text{on}1} r_1}{T_S N_1^2} + \frac{T_{\text{on}2} r_2}{T_S N_2^2} + \frac{T_{\text{off}} r_o}{T_S}. \tag{4}$$

B. Steady-State Characteristics

Removing the ideal transformers in the continuous equivalent circuit model in Fig. 6 and considering its steady state, the con-

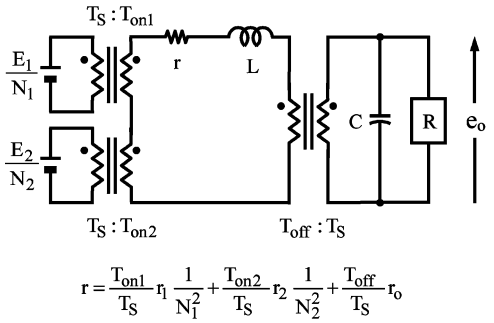

Fig. 6. Continuous equivalent circuit model averaged over a single switching period T_S.

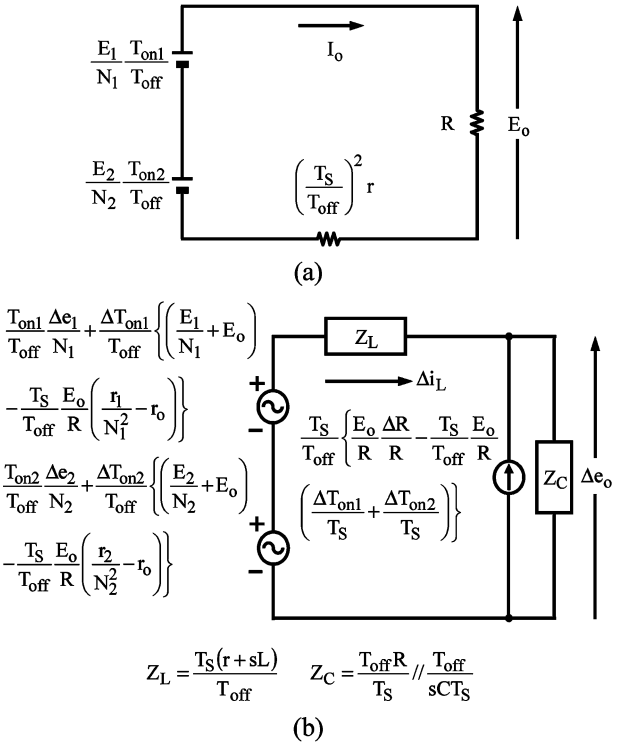

Fig. 7. (a) Continuous dc averaged model. (b) Continuous ac averaged model.

tinuous dc averaged model of the two-input dc–dc converter in Fig. 3(a) is derived and represented by Fig. 7(a). From Fig. 7(a), the steady-state characteristics are given by

$$E_o = \frac{E_1 \frac{T_{on1}}{(N_1 T_{off})} + E_2 \frac{T_{on2}}{(N_2 T_{off})}}{1 + \frac{r {T_S}^2}{({T_{off}}^2 R)}} \tag{5}$$

$$N_1 I_1 = I_o \frac{T_{on1}}{T_{off}} \tag{6}$$

$$N_2 I_2 = I_o \frac{T_{on2}}{T_{off}} \tag{7}$$

where I_o is the load current, while $N_1 I_1$ and $N_2 I_2$ are the input currents normalized by the turns ratio.

C. Dynamic Characteristics

In the multiple-input dc–dc converter, the circuit operation may become unstable since this converter is fundamentally composed of buck–boost-type circuits. Therefore, we will analyze here the boundaries of stability. Removing the ideal transformers

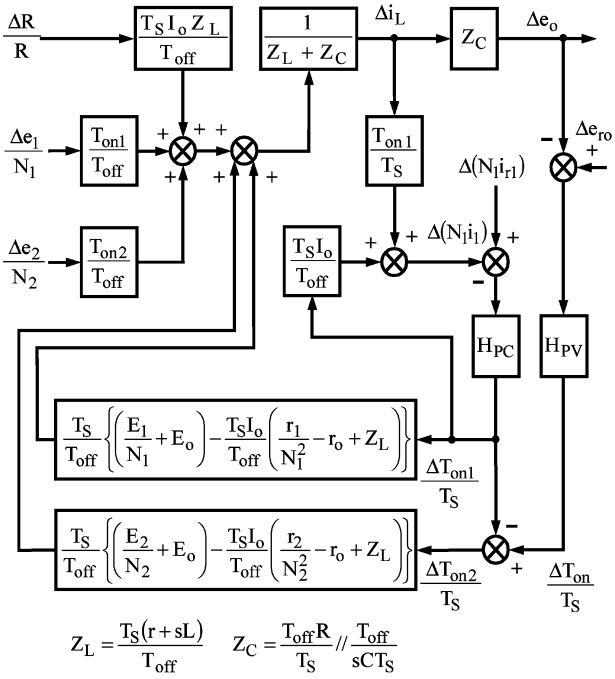

Fig. 8. Transfer function representation.

in Fig. 6 and considering the small ac variation from its equilibrium operating point, the ac averaged model of the two-input dc–dc converter can be derived and is shown in Fig. 7(b). In this figure, ΔT_{on1}, ΔT_{on2}, Δe_1, Δe_2, Δe_o, and ΔR are the small ac variations of the on time T_{on1}, T_{on2}, the input voltage E_1, E_2, the output voltage e_o, and the load resistance R, respectively. From Fig. 7(b), the transfer function representation of the two-input dc–dc converter can be derived as shown in Fig. 8. In this figure, H_{PC} and H_{PV} are the dc current gain of the controller #1 and the dc voltage gain of the controller #2 in Fig. 3(b). $\Delta T_{\rm on} = \Delta T_{\rm on1} + \Delta T_{\rm on2}$. $\Delta(N_1 i_1)$, $\Delta(N_1 i_{r1})$, and Δe_{ro} are the small ac variations of the input current $N_1 I_1$, reference input current $N_1 I_{r1}$, and reference output voltage E_{ro}, respectively. $\Delta T_{on}/T_S = -H_{PV}(\Delta e_o - \Delta e_{ro})$ and $\Delta T_{\rm on1}/T_S = -H_{PC}(\Delta N_1 i_1 - \Delta N_1 i_{r1})$. Applying the Routh–Hurwitz criterion, the following relation is obtained as the stable condition:

$$H_{PV} < \frac{T_{off}}{T_S E_o}\left(1 + \frac{r^* RC}{L}\right). \tag{8}$$

In (8), r^* is given by

$$r^* = r + \frac{N_1 I_1 \frac{T_{off}}{I_o T_S}}{\frac{1}{H_{PC}} + \frac{T_S I_o}{T_{off}}} \bullet \left\{\frac{E_2}{N_2}(G-1) - \frac{T_S I_o}{T_{off}}\left(\frac{r_1}{N_1^2} - \frac{r_2}{N_2^2}\right)\right\} \tag{9}$$

where G is given by

$$G = \frac{\frac{E_1}{N_1}}{\frac{E_2}{N_2}}. \tag{10}$$

G represents the normalized input voltage ratio of E_1 and E_2. The relation (8) as the stable condition coincides with that of the conventional buck–boost-type dc–dc converter with an single input source if r^* might be its equivalent internal loss resistance.

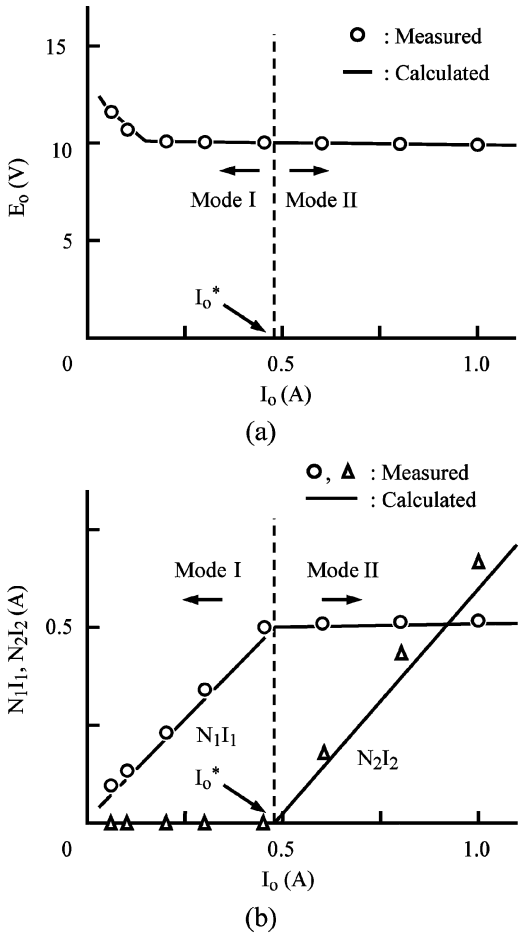

Fig. 9. Regulation characteristics ($E_2/N_2 = 10$ V, $G = 1$, $L = 0.4$ mH, $C = 4000\ \mu$F, $r = r_1/N_1^2 = r_2/N_2^2 = r_o = 0.2\ \Omega$, $H_{PC} = 30\ A^{-1}$, $H_{PV} = 0.117\ V^{-1}$). (a) Output voltage E_o for the change of the load current I_o. (b) Input currents N_1I_1 and N_2I_2 for the change of I_o.

IV. Experiment and Discussion

Fig. 9(a) shows the regulation characteristics of the output voltage E_o for the change of the load current I_o. In this figure, the solid line and symbol ○ indicate the theoretical and experimental results, respectively. Fig. 9(b) shows the input currents N_1I_1 and N_2I_2 for the change in I_o. In this figure, the symbols ○ and Δ indicate the experimental values of N_1I_1 and N_2I_2, respectively, and the solid lines indicate the theoretical ones. Mode I and Mode II are in the left and right regions of the broken line, respectively. Under the boundary condition between Mode I and Mode II, T_{on2} is equal to zero and, thus, T_{on1} is equal to $T_S - T_{\text{off}}$. Taking account of (5), (6), (7), and $T_{\text{on1}} = T_S - T_{\text{off}}$, the load current I_o^* under the boundary condition between Mode I and Mode II is derived as follows:

$$I_o^* = -\frac{\left\{N_1I_1\left(\frac{r_1}{N_1^2}+r_o\right)+E_o\right\}}{2r_o} + \left[\frac{\left\{N_1I_1\left(\frac{r_1}{N_1^2}+r_o\right)+E_o\right\}^2}{4r_o^2} + \left\{\frac{E_1}{N_1}-\left(\frac{r_1}{N_1^2}\right)N_1I_1\right\}N_1\frac{I_1}{r_o}\right]^{0.5}. \quad (11)$$

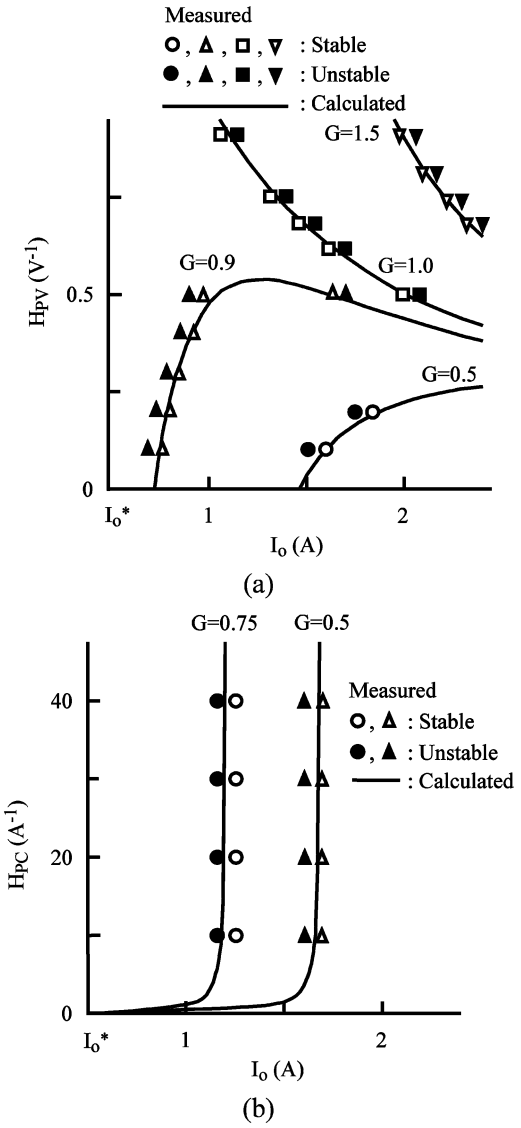

Fig. 10. Boundaries of stability ($L = 0.4$ mH, $C = 4000\ \mu$F, $r = r_1/N_1^2 = r_2/N_2^2 = r_o = 0.2\ \Omega$, $E_2/N_2 = 10$ V, $N_1I_1 = 0.5$ A). (a) With respect to the dc voltage gain H_{PV} ($H_{PC} = 30\ \text{A}^{-1}$, $E_o = 10$ V). (b) With respect to the dc current gain H_{PC} ($H_{PV} = 0$, $T_{\text{off}}/T_S = 0.5$).

Under the light-load condition, the two-input converter works in Mode I and the output current I_o is supplied as N_1I_1 shown in Fig. 9(b) from the solar array in Fig. 3. In Mode I, N_1I_1 is proportional to I_o as shown in Fig. 9(b). When I_o is larger than I_o^*, this converter works in Mode II. In Mode II, employing the maximum power tracker of the solar array, the input current N_1I_1 can be restricted to track the optimum power point of the solar array E_1, and the shortage of the load power is supplied as the input current N_2I_2 from E_2. As shown in Fig. 9, the calculated values agree well with the measured ones, and the output voltage E_o is sufficiently regulated in Mode I and Mode II.

Fig. 10(a) shows the boundaries of stability concerning the dc voltage gain H_{PV} of the controller #2 in Fig. 3(b). In Fig. 10, the solid lines indicate the theoretical boundaries of stability calculated by (8)–(10), taking the normalized input voltage ratio G. In Fig. 10(a), ○, Δ, □, and ∇ indicate the measured points in the

stable region in the case of $G = 0.5$, 0.9, 1.0 and 1.5, respectively. ●, ▲, ■, and ▼ indicate the measured points in unstable region in the case of $G = 0.5$, 0.9, 1.0 and 1.5, respectively. The theoretical values agree well with the experimental ones. H_{PV} can be enlarged with an increase in G. In this figure, the dc current gain H_{PC} of the controller #1 in Fig. 3(b) is equal to $30\,\mathrm{A}^{-1}$). In particular, when H_{PV} is equal to zero, the boundaries of stability concerning H_{PC} are shown in Fig. 10(b). In this figure, ○ and △ indicate the measured points in the stable region in the case of $G = 0.75$ and 0.5. It is important to note that the operation of the two-input dc–dc converter becomes unstable when G is less than unity and the output voltage is not fed back, and that the stable region is enlarged with an increase in G. When G is larger than unity, the circuit operation is always stable.

V. Conclusion

The new multiple-input dc–dc converter has been proposed to combine and exploit several clean energy sources. Furthermore, the two-input dc–dc converter using magnetic coupling of the reactor was analyzed theoretically and experimentally. As a result, the following points are clarified.

1) In the two-input dc–dc converter system, where a solar array and a commercial ac line are used as two-input power sources, the output voltage can be regulated by receiving adequate power from the commercial ac line, even if the load is changed.
2) The dynamic characteristics, in particular, those of the boundaries of stability, are clarified. If circuit parameters are designed adequately the proposed converter is sufficiently stable and useful.

We will extend this analysis from the two-input to the multiple-input and also the forward-type converter in the near future.

Appendix I
States of Behavior and Operation Modes

There exist eight states according to the combination of the on and off conditions of the switches S_1, S_2 and diode D. However, considering the electrical circuit theory, four states are invalid except for four states shown in Table I. In State 1, S_1 is on, S_2 is off, and D is off. In this state, the current I_1 flows from E_1 to the winding N_1 of the reactor L through R_S, D_1 and S_1, and then the magnetic energy is stored in L in Fig. 3(b). In State 2, S_1 is off, S_2 is on, and D is off. In this state, the current I_2 flows from E_2 to the winding N_2 of L through D_2 and S_2, and the energy is stored in L. In State 3, S_1 is off, S_2 is off, and D is on. In this state, the current flows from the secondary winding of L to the load R connected with the output capacitor C in parallel through D and the stored energy in State 1 and/or State 2 are transferred to R. In State 4, S_1 is off, S_2 is off, and D is off. In this state, I_1, I_2, and the secondary winding current do not flow at all, and the discharged current flows from C to R. There exist six operation modes by combining these four states. Considering the electric energy flows from E_1 and E_2 to the load, the operation of the converter is divided into three major modes. The electric energy flows from only E_1 or E_2 to the load in Mode I or Mode III, respectively. In Mode II, the energy flows from both of E_1 and E_2 to the load.

Appendix II
Derivation of the Continuous Equivalent Circuit Model Averaged Over a Single Switching Period T_S Shown in Fig. 6

First, as to the ideal transformer in Fig. 5, let us transform turns ratios of 1:1, 1:0, and 0:1 in State 1, 1:0, 1:1, and 0:1 in State 2, and 1:0, 1:0, and 1:1 in State 3 into those of $T_{\mathrm{on1}} : T_{\mathrm{on1}}$, $T_{\mathrm{on1}} : 0$, and $0 : T_{\mathrm{on1}}$ in State 1, $T_{\mathrm{on2}} : 0$, $T_{\mathrm{on2}} : T_{\mathrm{on2}}$, and $0 : T_{\mathrm{on2}}$ in State 2, and $T_{\mathrm{off}} : 0$, $T_{\mathrm{off}} : 0$, and $T_{\mathrm{off}} : T_{\mathrm{off}}$ in State 3, respectively, because the time intervals of State1, State 2, and State 3 are T_{on1}, T_{on2}, and T_{off}, respectively. Next, superimposing transformed three equivalent circuits with the same topology corresponding to State 1, State 2, and State 3 in Fig. 5, the continuous equivalent circuit model averaged over a single switching period T_S is derived.

Acknowledgment

The authors wish to express their appreciation to Dr. Y. Ishizuka and M. Kawahara of Nagasaki University for their assistance.

References

[1] H. Matsuo *et al.*, "Analysis of multi-input dc-dc converter for natural energy conversion," in *Proc. 1992 Annu. Conf. Institute of Electronics Information and Communication Engineers of Japan*, Mar. 1992, p. 345.
[2] H. Matsuo and N. Watanabe, "DC-DC converter," Japanese Patent 2 502 238, Mar. 31, 1996.
[3] H. Matsuo and F. Kurokawa, "New solar cell power supply system using a boost type bidirectional dc-dc converter," *IEEE Trans. Ind. Electron.*, vol. IE-31, pp. 51–55, Feb. 1984.
[4] G. W. Wester and R. D. Middlebrook, "Low-frequency characterization of switched dc-dc converters," *IEEE Trans. Aerosp. Electron. Syst.*, vol. AES-9, p. 376, May 1973.

Hirofumi Matsuo (SM'88–F'00) was born in Fukuoka, Japan, in 1946. He received the B.E. degree from the University of Osaka Prefecture, Sakai-shi, Japan, in 1969, and the M.E. and Dr. Eng. degrees from Kyusyu University, Fukuoka-shi, Japan, in 1971 and 1977, respectively.

Currently, he is a Professor in the Graduate School of Science and Engineering, Nagasaki University, Nagasaki, Japan. His research interests are switching converters, inverters, and active filters, and high-speed digital signal processing. In 2001, he established the 173rd Committee "Information and Communication Switching Power Supply Systems in the Next Era" of Japan Society for the Promotion of Science, as an industry–university research corporation committee which is composed of 40 university members and 40 industry members.

Dr. Matsuo is a Member of the Institute of Electrical Engineers of Japan, Illuminating Engineering Institute of Japan, Institute of Image Information and Television Engineers of Japan, and Magnetics Society of Japan. He received the Ohm Technical Award for contributions to the research and development of switching power electronic circuits in 1999.

Wenzhong Lin received the B.E. and M.E. degrees from Fuzhou University, Fuzhou, China, in 1987 and 1990, respectively. He is currently working toward the Dr. Eng. degree in the Graduate School of Science and Technology, Nagasaki University, Nagasaki, Japan.

From 1991 to 1998, he was a Lecturer at Minjiang University, China. From 1998 to 1999, as a Visiting Researcher, studying switching power converters, at Nagasaki University, Japan. His main research interest is in the area of switching power converters.

Fujio Kurokawa (M'93–SM'02) was born in Yamaguchi, Japan, in 1952. He received the B.S. degree in electronic engineering from Fukuoka Institute of Technology, Fukuoka, Japan, in 1976, and the Dr. Eng. degree from Osaka Prefecture University, Sakai, Japan, in 1988.

From 1977 to 1984, he was a Teaching Fellow at Fukuoka Institute of Technology. Since 1984, he has been with the Faculty of Engineering, Nagasaki University, Nagasaki, Japan, where he is currently an Associate Professor of Electrical and Electronic Engineering. His research and teaching interests are in the areas of electronic circuits, power electronics, robotics, and image processing systems.

Dr. Kurokawa is a Senior Member of the IEEE Power Electronics Society, Institute of Electronics, Information and Communication Engineers of Japan, Institute of Electrical Engineers of Japan, Illuminating Engineering Institute of Japan, Institute of Image Information and Television Engineers of Japan, and the Information Processing Society of Japan.

Tetsuro Shigemizu received the B.E. and M.E. degrees from Nagasaki University, Nagasaki, Japan, in 1987 and 1989, respectively.

Since 1989, he has been with the Nagasaki Research and Development Center, Mitsubishi Heavy Industries, Ltd., Nagasaki, Japan.

Mr. Shigemizu is a Member of the Institute of Electrical Engineers of Japan.

Nobuya Watanabe graduated from Chiba Institute of Technology, Chiba, Japan, in 1954.

From 1969 to 1972, he was a Visiting Researcher and Auditor in the Department of Electronics, Kyushu University, Japan. He was with Mitsubishi Heavy Industry Company, Ltd. from 1954 to 1993. Since 1994, he has been with Choryo Engineering Company, Ltd., Nagasaki, Japan, as a Technical Adviser.

Mr. Watanabe is a Member of the Institute of Electrical Engineers of Japan.